scientific reports

Check for updates

OPEN

Recording site placement on planar silicon-based probes affects signal quality in acute neuronal recordings

Richárd Fiáth[1,2]✉, Domokos Meszéna[1,2], Zoltán Somogyvári[3], Mihály Boda[2], Péter Barthó[1], Patrick Ruther[4,5] & István Ulbert[1,2]

Multisite, silicon-based probes are widely used tools to record the electrical activity of neuronal populations. Several physical features of these devices are designed to improve their recording performance. Here, our goal was to investigate whether the position of recording sites on the silicon shank might affect the quality of the recorded neural signal in acute experiments. Neural recordings obtained with five different types of high-density, single-shank, planar silicon probes from anesthetized rats were analyzed. Wideband data were filtered to extract spiking activity, then the amplitude distribution of samples and quantitative properties of the recorded brain activity (single unit yield, spike amplitude and isolation distance) were compared between sites located at different positions of the silicon shank, focusing particularly on edge and center sites. Edge sites outperformed center sites: for all five probe types there was a significant difference in the signal power computed from the amplitude distributions, and edge sites recorded significantly more large amplitude samples both in the positive and negative range. Although the single unit yield was similar between site positions, the difference in spike amplitudes was noticeable in the range corresponding to high-amplitude spikes. Furthermore, the advantage of edge sites slightly decreased with decreasing shank width. Our results might aid the design of novel neural implants in enhancing their recording performance by identifying more efficient recording site placements.

To investigate the biological mechanisms behind complex brain functions (e.g. memory, sensation or consciousness) we have to monitor and manipulate the dynamics of neural populations of a statistically representative size, comprising hundreds or even thousands of neurons[1,2]. Current research methods able to record the activity of that many individual cells simultaneously are extracellular electrophysiological recordings[3–8] and optical imaging techniques (e.g. two-photon calcium imaging[7,9–11]). Although most brain imaging approaches provide high spatial resolution, due to the slow kinetics of calcium indicators and limitations in the imaging speed, their temporal resolution is often low compared to electrophysiological techniques[12,13]. This might hinder the precise registration of the action potential firing times of single cells, especially if the activity of many neurons is measured simultaneously. In contrast, recently developed high-density silicon-based multielectrode arrays[3–6,14–19] can monitor the activity of hundreds of neurons at the same time with sub-millisecond precision and, because of the large number of closely packed recording sites, also with a high spatial resolution.

Planar silicon-based neural probes, which currently are among the most frequently used microelectrode types applied to measure extracellular brain activity, are fabricated using microelectromechanical system (MEMS) and complementary metal–oxide–semiconductor (CMOS) microtechnology. These methods allow to precisely realize the physical and geometrical parameters of these devices as well as to add integrated circuits on the probe shank or base for on-chip signal conditioning[20]. Considering the findings of previous research using neural implants for acute and chronic electrophysiological recordings, several features of silicon microprobes are now designed to minimize the mechanical trauma caused during probe insertion as well as to enhance their recording

[1]Institute of Cognitive Neuroscience and Psychology, Research Centre for Natural Sciences, Budapest, Hungary. [2]Faculty of Information Technology and Bionics, Pázmány Péter Catholic University, Budapest, Hungary. [3]Department of Computational Sciences, Wigner Research Centre for Physics, Budapest, Hungary. [4]Department of Microsystems Engineering (IMTEK), University of Freiburg, Freiburg, Germany. [5]Cluster of Excellence, BrainLinks-BrainTools, University of Freiburg, Freiburg, Germany. ✉email: fiath.richard@ttk.hu

performance, both for the short and long term. For instance, in earlier studies it has been shown that the shank size of the neural implant has a significant impact on the extent of tissue damage caused by the insertion or on chronic tissue response[21–23]. Furthermore, the shape of the probe tip or the implant tethering may also affect the quality of the recorded neural signals in the long term[24–26]. Besides physical features of these neural devices, the conditions of probe insertion (e.g. insertion speed or alignment of the probe) might also have a notable effect on the recording performance[24,27–29].

An essential part of neural probes are the small recording sites which detect the electrical activity of neurons and are placed commonly on one of the sides of the silicon shank. The influence of size, impedance and material of recording sites on neural recordings is relatively well studied[30–33]. However, prior research investigating the optimal placement of recording sites on silicon shanks to achieve high quality recordings is scarce and does not provide an in-depth analysis of this topic[34–36]. In chronic experiments, Lee and colleagues found that recording sites placed on the edge of planar silicon probes perform slightly better than center sites[35]. The difference in signal quality was significant for wide (249 µm) devices but smaller and not significant for narrower (132 µm) probes. In contrast, the study of Scott and colleagues found no significant effect of site position on the recording quality in acute experiments[34]. However, in their study they only used data from one type of silicon probe (having an 85-µm-wide shank) and did not perform spike sorting to separate the action potentials of individual neurons. Evaluating data obtained with a polymer-based probe having a special edge electrode design showed a higher single unit yield and larger signal amplitudes on edge electrodes compared to sites located on the front side of the parylene shank[36]. Although edge sites outperformed the recording performance of other site positions, only a small number of recordings were analyzed in the study and signal amplitudes were only qualitatively compared.

As silicon probes and electrophysiological recording devices become affordable for more and more labs, which process is further accelerated by the open source movement[37–40], it is an important mission to thoroughly study various features of neural probes as well as brain-implant interactions to aid the design of future devices with the goal of enhancing their recording capabilities. An optimal placement of recording sites on planar silicon probes might increase the signal quality as well as the single unit yield significantly, and thereby decrease the costs and time requirements of electrophysiological experiments. Recording sites on commercially available passive silicon probes are usually placed in the center of the shank, although several variants of probes with edge sites also exist[41]. Contrary to that, recently developed silicon probes with high electrode density (e.g. the Neuropixels probe) contain sites both near the edge and in the center of their shank[3,4,14,18,42]. This site configuration provides an excellent opportunity to compare the recording performance of various site positions. In this comprehensive quantitative study, our aim was to examine whether the location of recording sites on high-density, single-shank, planar silicon-based probes might affect the quality of the recorded neural activity on acute timescales. In order to investigate this question, we examined electrophysiological recordings obtained from the neocortex of anesthetized rats with multiple probe types having different shank widths. Recording sites were labeled as edge or center sites according to their position on the silicon shank, then we analyzed the amplitude distribution of the recorded signal as well as various properties of single unit activity (e.g. single unit yield, peak-to-peak amplitude of single unit spike waveform) separately on these two site groups.

Methods

Silicon probe types. Neural recordings obtained with five different types of silicon-based, single-shank planar probes were analyzed in this study[3,14,42] (Fig. 1). These probes have different shank widths (ranging from 50 to 125 µm), shank thicknesses (from 20 to 50 µm) and recording site features. All selected probe types have a high number of closely packed recording sites, ranging from 32 to 960 sites. To be able to make a reliable comparison in terms of site position, we only chose probes that contained recording sites both near the edge and the center of their silicon shank. Details of the features of these probes are listed below.

The device with the lowest channel count was a commercially available silicon probe (A1 × 32-Poly3-10 mm-50-177; NeuroNexus Technologies; www.neuronexus.com) with 32 iridium microelectrodes having a diameter of 15 µm (site area: 177 µm^2), and a center-to-center distance of 50 µm (Fig. 1a). The silicon shank of the probe is 10 mm long and has a cross-section of 125 µm × 50 µm [Width (W) × Thickness (T)] at the level of the recording sites. The circular sites are arranged in three equidistantly spaced columns with one column located on each side of the shank (edge sites) and the third column in the center (center sites). The edge columns contain 10 microelectrodes each while the center column comprises 12 sites. The brain area covered by the recording sites is approximately 125 µm × 550 µm [W × Length (L)]. The lowermost site (center column) is located 100 µm far from the probe tip. The closest point of edge sites from the edge of the silicon shank is 5 µm. This probe type is frequently used to record spiking activity from rats and mice[27,43–45], was applied as mesh model in a computational modeling study[46], and was also used in the evaluation of the effect of site impedance on neural data quality[30].

The second device was a 128-site silicon probe with closely spaced low-impedance titanium nitride electrodes recently developed in the NeuroSeeker research project[14] (www.neuroseeker.eu; Fig. 1b). This type of multielectrode has an 8 mm long shank with a cross-section of 100 µm × 50 µm (W × T). The spacing between the edges of the square-shaped recording sites (20 µm × 20 µm; site area: 400 µm^2) is 2.5 µm. The sites are arranged in four equidistantly spaced columns (one column on each side and two columns in the center of the silicon shank) with all columns containing 32 microelectrodes. One microelectrode located at the top row on the right side has a larger area and serves as an internal reference electrode (only partially shown in Fig. 1b). The bottom row of recording sites is located 300 µm far from the chisel-shaped probe tip. The array of microelectrodes covers an area of 87.5 µm × 717.5 µm (W × L). The side of edge sites is approximately 6.25 µm far from the edge of the silicon shank. The 128-channel probe provides high-quality neural signals in acute experiments both from rodents and cats[14,27,43,47], and was also chronically implanted in monkeys[48].

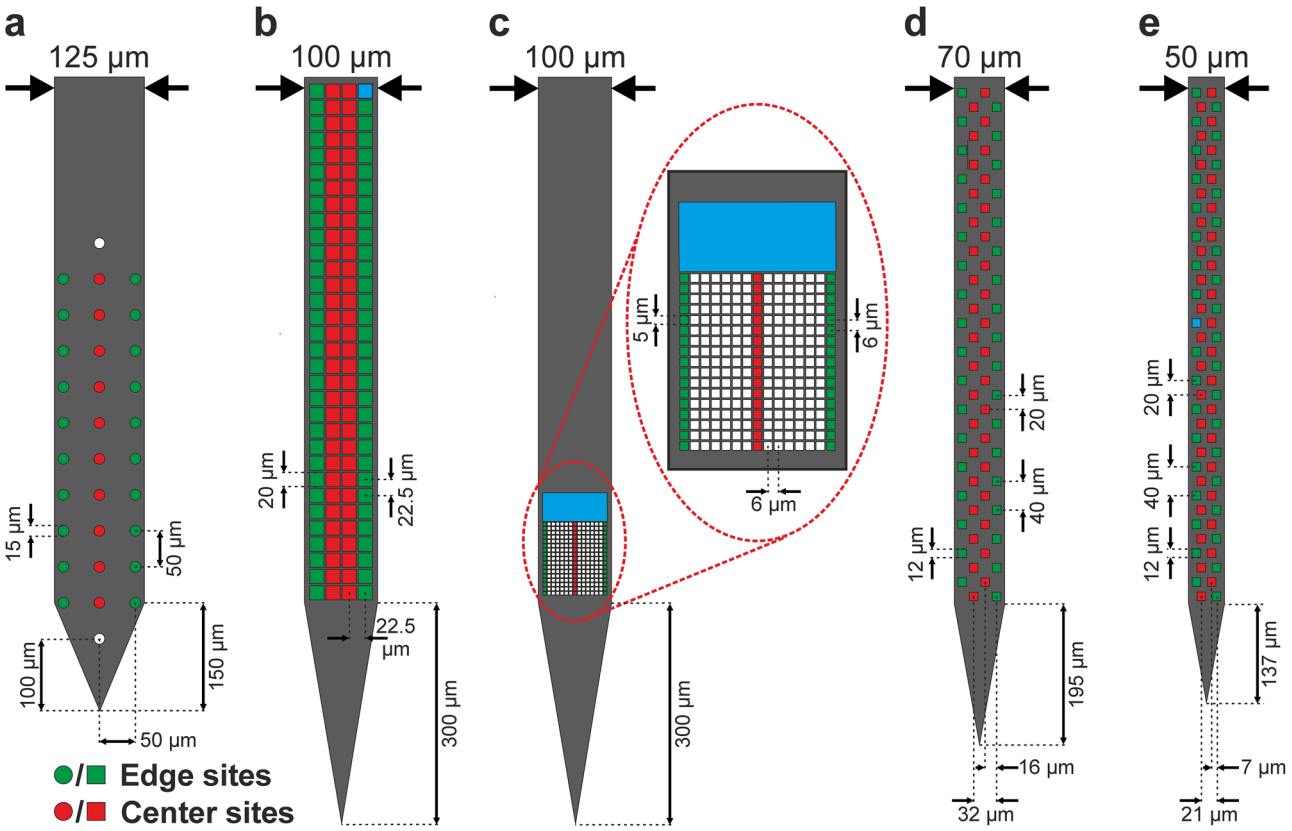

Figure 1. Schematic illustration of the five probe types examined in this study ordered by shank width. (**a**) 32-channel silicon polytrode (NeuroNexus). (**b**) 128-channel silicon probe (NeuroSeeker). (**c**) 255-channel silicon probe (NeuroSeeker). (**d**) Neuropixels probe with 70 µm shank width. (**e**) Neuropixels probe with 50 µm shank width. Recording sites classified as edge sites are colored green, while center sites are marked with red color. Sites colored white were either not located at the investigated positions or the data obtained by these were not used in the analysis. Blue sites on panel (**b**), (**c**) and (**e**) correspond to internal reference electrodes. Only a subset of recording sites is shown in the case of the Neuropixels probes.

The third probe type was also developed in the NeuroSeeker project using the same fabrication technology (Fig. 1c). It has 255 miniature quadratic titanium nitride recording sites (5 µm × 5 µm; site area: 25 µm^2). From this probe type, two different designs were fabricated, one with a linearly placed microelectrode array[49], and another with a closely packed array of 17 × 15 recording sites[42]. The latter version was used in this study. The silicon shank of this probe has the same parameters as described above for the 128-channel probe. The spacing between the edge of small recording sites is 1 µm (corresponding to a center-to-center electrode distance of 6 µm). The probe has a large internal reference site located above the small sites. The bottom row of microelectrodes is located 300 µm from the chisel-shaped probe tip. The array of microelectrodes covers an area of 89 µm × 101 µm (W × L).

The fourth and fifth devices are two variants of the recently developed Neuropixels CMOS-based silicon probe[3,50] (www.neuropixels.org; Fig. 1d,e). The commercially available version has a 10 mm long shank with a cross-section of 70 µm × 20 µm (W × T; Fig. 1d). It contains 960 square-shaped titanium nitride microelectrodes (12 µm × 12 µm; site area: 144 µm^2) from which 384 can be selected for recording. The recording sites are arranged in a checkerboard pattern with 4 columns and 480 rows. The center-to-center distance of microelectrodes in a single row is 32 µm. Alternate columns are offset by 16 µm and the vertical spacing of microelectrodes is 40 µm. The gap between the edge of the probe shank and the edge of the first recording sites is 5 µm. The center of the bottom row of sites is 195 µm away from the tip of the shank. The array of 384 adjacent recording sites covers a brain area of approximately 60 µm × 3800 µm (W × L). In addition, we analyzed data from a publicly available dataset obtained with another Neuropixels probe variant (PhaseA Option 1 probe[50]). This probe has a shorter shank (5 mm), a smaller shank width (50 µm) and only 384 recording sites arranged in 4 columns and 192 rows (Fig. 1e). The features of recording sites are the same as described above. The center-to-center distance of microelectrodes in a single row is 21 µm and alternate columns are offset by 7 µm. The vertical spacing of microelectrodes is 40 µm and the side of edge sites is located 5 µm from the edge of the silicon shank. The center of the bottom row of sites is 137 µm away from the tip of the shank. The brain area covered by the recording sites is approximately 40 µm × 3800 µm (W × L). Neuropixels probes are being increasingly used in electrophysiology labs and became essential tools of cutting-edge neuroscience research[6,51,52].

The probes investigated in this study were designed principally for acute in vivo recordings, although Neuropixels probes can be used for chronic experiments[53,54] and the 32-channel NeuroNexus probe is also available

Probe type	No. of recording sites	No. of channels in separated recordings	No. of analyzed recordings	No. of rats	No. of penetrations	Insertion speed (mm/s)	Type of anesthesia	Average recording length (min)	Reference
32-channel NeuroNexus probe (125 µm wide)	32	10	10	6	10	0.002	Ketamine/xylazine	31	www.neuronexus.com
128-channel NeuroSeeker probe (100 µm wide)	128	32	10	10	10	0.002	Ketamine/xylazine	30	14
Neuropixels probe (70 µm wide)	384	58	6	4	6	~1	Urethane	31	www.neuropixels.org
Neuropixels probe (50 µm wide)	384	58	7	6	7	0.005	Urethane	20	50
255-channel NeuroSeeker probe (100 µm wide)	255	17	21	2	2	0.002	Ketamine/xylazine	32	42, 49

Table 1. Details of the experiments and recordings of the five silicon probe types.

with a chronic design. Except for the NeuroNexus probe, all probes were fabricated using a 0.13-µm CMOS fabrication process. All probe types are passive devices, except for the Neuropixels probes which contain on-chip electronics for signal conditioning (e.g. for filtering, amplification or multiplexing) and digitization on the probe[3]. Electrical impedance of titanium nitride sites of CMOS-fabricated probes was low (< 1 MΩ at 1 kHz) but varied between different probe types due to the difference in the area of recording sites. However, the absolute impedance magnitude values of a particular probe type showed low variability[3,14,49] (about a few kΩ). The site impedance of the NeuroNexus probe measured at 1 kHz was 385.63 kΩ ± 30.7 kΩ (mean ± standard deviation; average of 64 recording sites of two probes). No statistically significant difference was found between the impedance of edge and center sites of the examined probe types.

Analyzed datasets. To obtain data for analysis, we performed acute experiments in anesthetized rats and recorded spontaneously occurring cortical activity with each probe type (see sections "Animal surgery" and "Electrophysiological recordings" below for details), except for the Neuropixels probe with 50 µm shank width. In the latter case, recordings from a publicly available online database were used for analysis[50] (n = 7 out of 43 files with the following file identifiers: c5, c8, c12, c24, c26, c32, c45). All public Neuropixels data files were visually inspected to select recordings with the best quality. To avoid data redundancy, only one recording file was used from a particular dataset which contained multiple recordings measured from the same penetration. A subset of the 128-channel probe data analyzed here originated from the dataset obtained in another study[27]. Details of the recordings per probe type can be found in Table 1.

Publicly available cortical recordings (n = 7) acquired by the 255-channel NeuroSeeker probe were also analyzed in this work[42] (recordings with the following identifiers were used: Co1-Co3, Co5 and CoP1-CoP3; www.kampff-lab.org/ultra-dense-survey; Supplementary Table 1). However, because of differences in the experimental conditions and data quality, these public recordings and our 255-channel measurements were assessed separately.

To examine the effect of sample size on the results, a larger cortical dataset acquired during previous projects (e.g. Refs.[14,27]) with the 128-channel probe was also included for analysis. A total of 179 recordings (n = 41 rats and ~ 100 penetrations) with durations ranging from 5 to 45 min were examined. The recordings contained activity from each layer of the rat cortex.

To examine the differences in signal quality between edge and center sites in another brain structure, a small dataset obtained from the thalamus was also evaluated (n = 9 recordings; Supplementary Table 2).

Animal surgery. All experiments were performed according to the EC Council Directive of September 22, 2010 (2010/63/EU), and all procedures were reviewed and approved by the Animal Care Committee of the Research Centre for Natural Sciences and by the National Food Chain Safety Office of Hungary (license number: PEI/001/2290-11/2015). The study was carried out in compliance with the ARRIVE guidelines. In the case of the 32-channel, 128-channel and 255-channel probe types, acute in vivo experiments were carried out similarly as described in our earlier studies[14,27,49]. In short, Wistar rats were anesthetized with a mixture of ketamine (75 mg/kg of body weight) and xylazine (10 mg/kg of body weight) injected intramuscularly. If necessary, supplementary ketamine/xylazine injections were given to maintain the depth of anesthesia during surgery and recordings. The animals were placed in a stereotaxic frame (David Kopf Instruments, Tujunga, CA, USA) after they reached the level of surgical anesthesia. The body temperature of rats was maintained with a homeothermic heating pad connected to a temperature controller (Supertech, Pécs, Hungary). After the removal of the skin and the connective tissue from the top of the skull, a craniotomy with a size of about 3 × 3 mm^2 was drilled over the neocortical area of interest (trunk region of the somatosensory cortex (S1Tr); approximate coordinates of the target site were: anterior–posterior (AP): – 2.7 mm; medial–lateral (ML): 2.5 mm; with respect to the bregma[55]). Then, to avoid excessive brain dimpling during the insertion of the single-shank silicon probes, a small slit was carefully made

in the dura mater above the insertion site using a 30-gauge needle. In the case of the 32-channel and 128-channel probes, for a post-mortem histological verification of the recording location of the probe[56], the silicon shank was coated with red-fluorescent dye 1,1-dioctadecyl-3,3,3,3-tetramethylindocarbocyanine perchlorate (DiI, D-282, ~ 1% in absolute ethanol, Thermo Fischer Scientific, Waltham, MA, USA) before insertion. After that, the silicon probe mounted on a motorized stereotaxic micromanipulator (Robot Stereotaxic, Neurostar, Tübingen, Germany) was driven into the brain tissue with a slow insertion speed of 2 μm/s to decrease tissue damage[27]. Before electrophysiological recordings started, we allowed 15 min for the brain tissue to settle around the probe. During probe insertion, care was taken to avoid damaging blood vessels located on the brain surface. With the 32-channel and 128-channel probes, neural activity was recorded mostly from cortical layers where the neuronal spiking activity is the strongest during ketamine/xylazine-induced slow wave activity[57] (layers IV-V). However, the depth of recording varied slightly between penetrations. With the 255-channel probe, because it records only from a confined cortical region (~ 100 μm × 100 μm), we acquired during a single penetration data from multiple depths (using at least 100 μm insertion steps to avoid recording form overlapping areas) from cortical layers where spiking activity could be detected (layers III–VI). In the case of thalamic recordings acquired with the 128-channel probe, the probe was moved below the neocortex to a dorsoventral depth of about 4.5 mm–6.5 mm, to target somatosensory thalamic nuclei (the ventrobasal complex and the posterior nucleus). As in our prior studies, room temperature physiological saline solution was regularly dropped into the cavity of the craniotomy to prevent dehydration of the neocortex[14,27,49]. A stainless steel needle inserted in the neck muscle of the animal served as the reference and ground electrode during recordings[14,27,49].

In the case of the experiments with the 70-μm-wide Neuropixels probe, the rats were anesthetized using urethane (1.5 g/kg). The experimental procedure was similar as described above. The probes were driven into the parietal association cortex (AP: – 4.1 mm, ML: 3 mm; with respect to the bregma) by hand with a stereotaxic micromanipulator to a depth of ~ 3 mm, using an insertion speed of approximately 1 mm/s. After insertion, we waited 30 min before any recording. Details of experiments and recordings are summarized in Table 1.

At the end of the experiments, probes were withdrawn and cleaned by immersing them into 1% Tergazyme solution (Sigma-Aldrich, St. Louis, MO, USA) for at least 30 min followed by rinsing with distilled water for about 2 minutes[14,27,49]. Animals were deeply anesthetized after the experiment, then killed by transcardiac perfusion of physiological saline solution (100 ml) followed by a fixative containing 4% paraformaldehyde in 0.1 M phosphate buffer (PB, pH 7.4, 250 ml). We verified the recording location of probes by histological examination of the fixed brain tissue in the same way as described in Ref.[27].

Electrophysiological recordings. For the three passive probe types, recordings were performed similarly as described in our previous studies[14,27,49]. In short, spontaneously occurring brain electrical activity was obtained using an Intan RHD-2000 electrophysiological recording system (Intan Technologies, Los Angeles, CA, USA). Two 128-channel amplifier boards were used in the case of the 255-channel probe, one 64-channel and two 32-channel amplifier boards were used in the case of the 128-channel probe, and a single 32-channel board was used with the 32-channel probe. The recording system was connected to a laptop via USB 2.0. Wideband signals (0.1–7500 Hz) were recorded using a sampling frequency of 20 kHz/channel and a resolution of 16 bit. About 30 min of multichannel neuronal data were collected at a single recording location. Data were saved to a local network attached storage device for offline analysis.

In the case of the 32-channel probe, two probes were used for the experiments (n = 6 rats). One probe was implanted into the neocortex of five rats, while the other probe was used in one rat. One or two probe insertions were done in each animal (n = 10 penetrations in total). All recording sites of the probes were functional. Two identical probes from the same manufacturing batch were used during the experiments with the 128-channel probes[14,27]. Each probe was implanted in five rats (n = 10 penetrations in total). The probes contained a maximum of two unfunctional recording sites. Two penetrations were carried out with the 255-channel probe (n = 2 rats). The used probe had multiple unfunctional recording sites (n = 14 sites; the site map is shown in Supplementary Fig. 1a).

In the case of the Neuropixels probes, data recorded in the action potential band (AP, 300–10.000 Hz) was used. The sampling rate was 30 kHz/channel and digitization was performed at 10 bits, under a gain of 500, yielding a resolution of 2.34 μV per bit. Data was acquired using the SpikeGLX open-source software (github.com/billkarsh/SpikeGLX). The 70-μm-wide probe had one internal reference site, while the 50-μm-wide device had 12 internal reference electrodes.

Grouping of recording sites. Recording sites were either classified as edge or center sites based on their location on the silicon shank (Fig. 1 and Supplementary Fig. 2). For the 32-channel probe, the two columns of sites located on the sides of the shank were labeled as edge sites, and two 10-channel recording files were created from the original 32-channel data (edge sites; Fig. 1a). By removing the top and bottom recording sites (to match the channel number of files containing edge channels), we constructed a 10-channel recording file from the middle column of 12 sites (center sites; Fig. 1a). For the 128-channel probe, four 32-channel recording files were generated from the original 128-channel data based on the location of the columns of sites (Fig. 1b and Supplementary Fig. 2). Microelectrodes located on the sides were classified as edge sites while the sites in the two middle columns were categorized as center sites. For the 255-channel probe, the column of recording sites located on the left side of the probe were classified as edge sites, while sites in the 8th column were grouped as center sites, both containing 17 channels (Fig. 1c). The sites located on the right edge were not used in the analysis because of the high number of unfunctional channels (Supplementary Fig. 1a). In the case of the public 255-channel dataset, both edge columns were included in the analysis, as the number of bad sites was low on the edges (Supplementary Fig. 1b). For the Neuropixels probes, the assignment of site locations was similar as

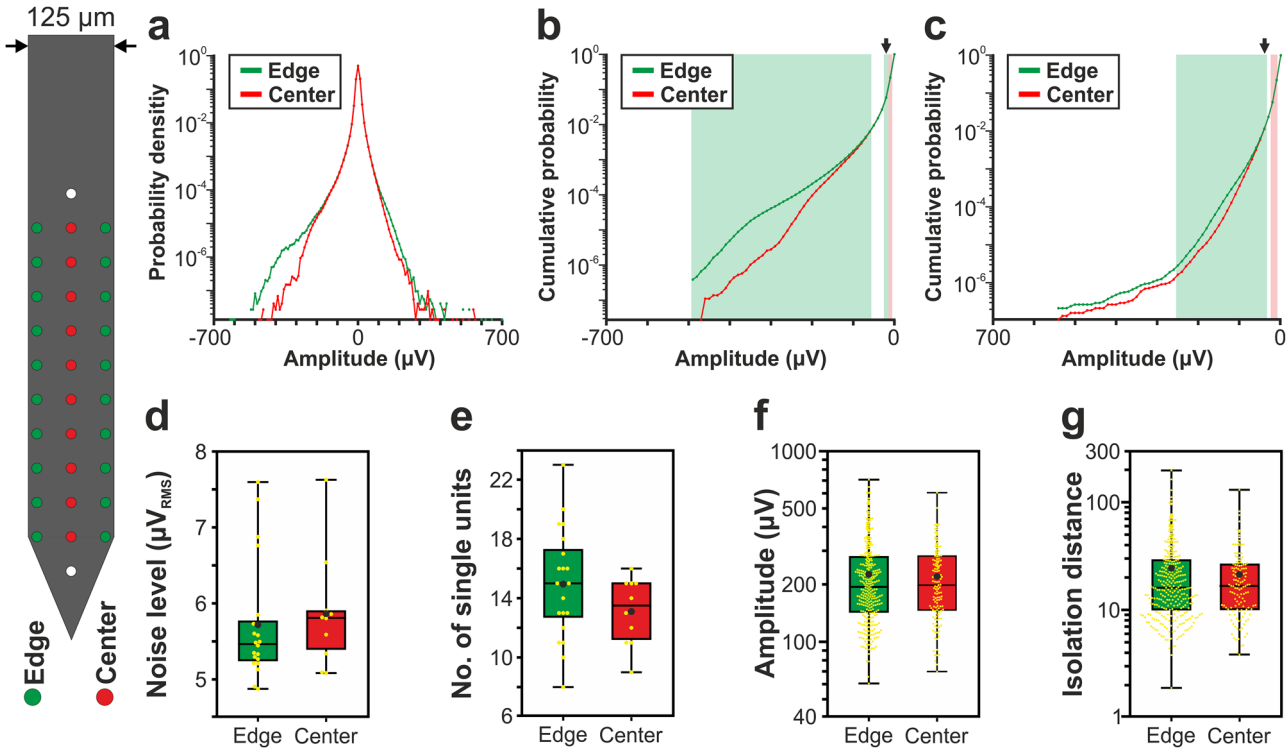

Figure 2. Comparison of the signal quality provided by edge (green) and center (red) sites of the 32-channel NeuroNexus silicon probe. (**a**) Probability density functions estimated from the amplitude of samples recorded in the 500–5000 Hz frequency range (n = 10 recordings). Probability values lower than 10^{-9} are not shown. (**b**) Cumulative distributions of amplitudes calculated in the negative amplitude range. (**c**) Reverse cumulative distributions calculated in the positive amplitude range. Green (or red) shaded areas in (**b**) and (**c**) indicate amplitudes with significantly higher numbers of edge (or center) samples. Arrows mark the maximal amplitude for edge significance in the negative range (− 20 µV; below this amplitude 2.95% of all negative samples were recorded on edge sites and 2.93% on center sites) and the minimal amplitude in the positive range (40 µV; above this amplitude 0.59% of all positive samples were recorded on edge sites and 0.57% on center sites). (**d**) Estimated in vivo noise level. (**e**) Single unit yield (n = 430). (**f**) Peak-to-peak amplitude of the averaged single unit spike waveforms. (**g**) Isolation distance of the single unit clusters. In the boxplots, the middle line indicates the median, while the boxes correspond to the 25th and 75th percentile. Whiskers mark the minimum and maximum values. The average is depicted with a black dot, whereas individual values are indicated with smaller yellow dots. Note that most data are plotted on a logarithmic scale. Mann–Whitney *U* test was used in (**d**–**g**).

described for the 128-channel probe (Fig. 1d,e). After removing channels corresponding to internal reference electrodes and their neighbors, as well as recording sites located outside of the cortex, the constructed individual recording files had 58 channels each.

All analyses were performed separately on the new data files created based on the position of recording sites. Since there was no statistically significant difference in the single unit properties between left and right sides of the probes (although there may be some differences in the amplitude distributions), results of the analyses obtained on data files that belonged to the same site group (e.g. left edge and right edge sites) were pooled and are presented together. However, the supplementary material contains also the results obtained on all separate recordings (panels a–e of Supplementary Figs. 9–12; Supplementary Tables 3–6).

In the case of the recordings obtained with the 128-channel probe, 32-channel files were generated also based on the longitudinal positions of recording sites (Supplementary Fig. 17a).

All data were analyzed and visualized using custom written MATLAB (R2017a) or Python (version 3.7) based scripts. Open source software was used for spike sorting (see "Spike sorting and calculation of single unit properties" section for details).

Amplitude distribution of the filtered potential. Probability density functions (PDFs) were calculated from the amplitudes of samples of the filtered potential (500–5000 Hz, Butterworth 3rd-order bandpass filter, zero-phase shift) to examine the difference in the signal amplitudes between edge and center sites. Channels corresponding to internal reference electrodes as well as bad sites were excluded from the analysis. Every 50th sample on each channel was used to create the PDFs (resulting in several millions of samples per site position). Because spike-like events with amplitudes lower than − 1000 µV (or higher than 1000 µV) are usually the results of artifacts (although in rare cases recording sites can detect spikes with negative peak amplitudes below this threshold which are fired by neurons located very close to these sites), potential values below − 1000 µV (and

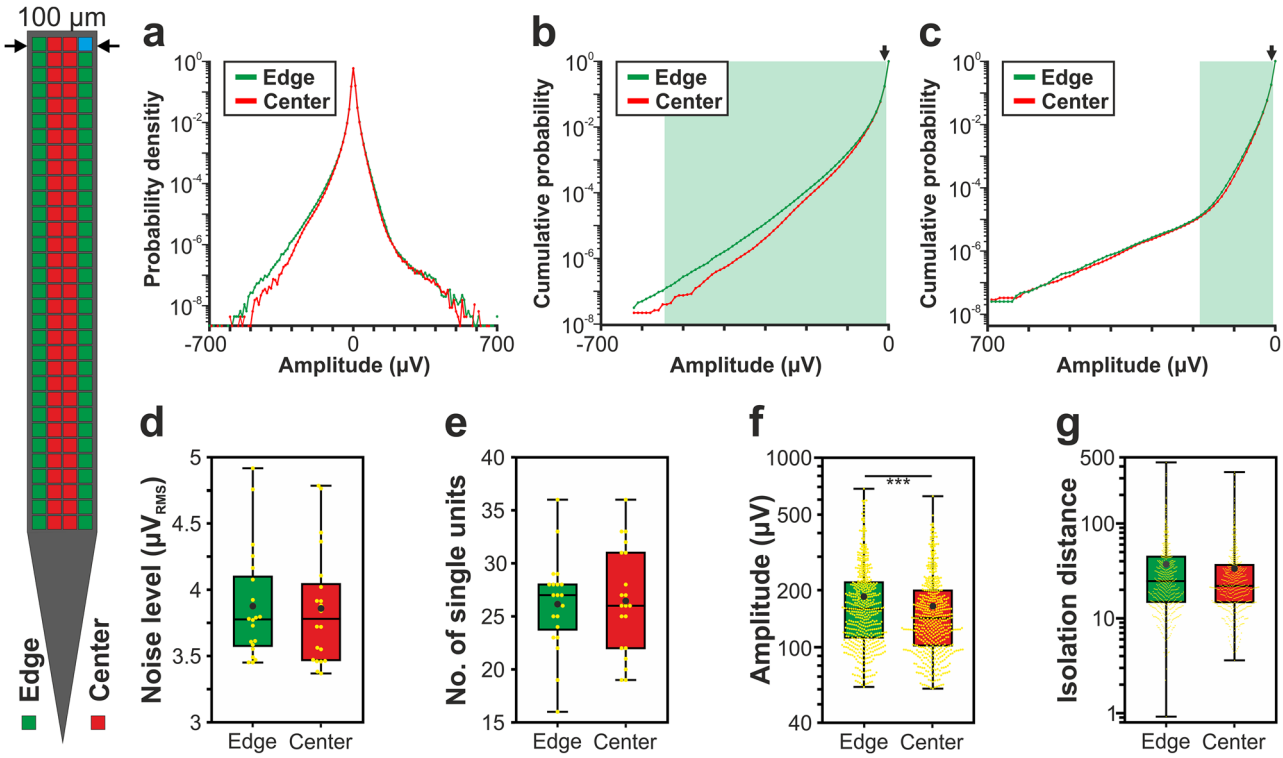

Figure 3. Comparison of the signal quality provided by edge (green) and center (red) sites of the 128-channel NeuroSeeker silicon probe. (**a**) Probability density functions estimated from the amplitude of samples recorded in the 500–5000 Hz frequency range (n = 10 recordings). Probability values lower than 10^{-9} are not shown. (**b**) Cumulative distributions of amplitudes calculated in the negative amplitude range. (**c**) Reverse cumulative distributions calculated in the positive amplitude range. Green shaded areas in (**b**) and (**c**) indicate amplitudes with significantly higher numbers of edge samples. Arrows mark the maximal amplitude for edge significance in the negative range (− 10 µV; below this amplitude 8.70% of all negative samples were recorded on edge sites and 8.64% on center sites) and the minimal amplitude in the positive range (10 µV; above this amplitude 9.02% of all positive samples were recorded on edge sites and 8.92% on center sites). (**d**) Estimated in vivo noise level. (**e**) Single unit yield (n = 1052). (**f**) Peak-to-peak amplitude of the averaged single unit spike waveforms. (**g**) Isolation distance of the single unit clusters. Note that most data are plotted on a logarithmic scale. Mann–Whitney U test was used in (**d**–**g**). ***$p < 0.001$.

above 1000 µV) were not examined here. For visualization purpose, very low probabilities ($p < 10^{-9}$) are not shown in the PDF plots (panel a of Figs. 2, 3, 4, 5 and 6). The signal quality was characterized and compared by means of total signal power, which was measured by the root mean square (RMS) amplitudes of the filtered data series.

After testing the total power differences between edge and center sites, we examined finer scale differences in the amplitude distributions, separately in the positive and in the negative amplitude ranges. For the negative amplitudes, the $P(a < x)$ cumulative amplitude distributions were calculated (panel b of Figs. 2, 3, 4, 5 and 6). The null hypotheses were that, given any x amplitude limit, the number of edge samples with amplitudes more negative than x follows a binomial distribution with probability $p_e = N_e/(N_e + N_c)$, where N_e is the number of samples from all the edge sites and N_c is the number of samples from all the center sites. The null hypothesis was rejected if there were significantly more edge samples below the amplitude x than it would be expected if edge and center samples would be chosen with the same probabilities. Finally, the maximal amplitude threshold can be identified with this method, below which the negative edge samples are more abundant, while above the threshold there are more center samples. The significant differences were calculated in the reverse direction as well, testing if the center samples are more abundant than the edge samples, by using $p_c = N_c/(N_e + N_c)$ probability for the binomial distributions.

For the positive values, the reverse cumulative distribution function was calculated as $P(a > x)$, and the same null hypotheses were rejected if the edge sample above the threshold x were significantly more abundant than the center samples (panel c of Figs. 2, 3, 4, 5 and 6). Then, the minimal x threshold was determined, above which there were more edge samples than center samples. Finally, the same tests were done to test the abundance of the center samples as well.

The full positive and negative amplitude ranges were divided and tested in 100 uniform steps. Considering the two directions, the 0.05 alpha values were Bonferroni-corrected for the 200 comparisons.

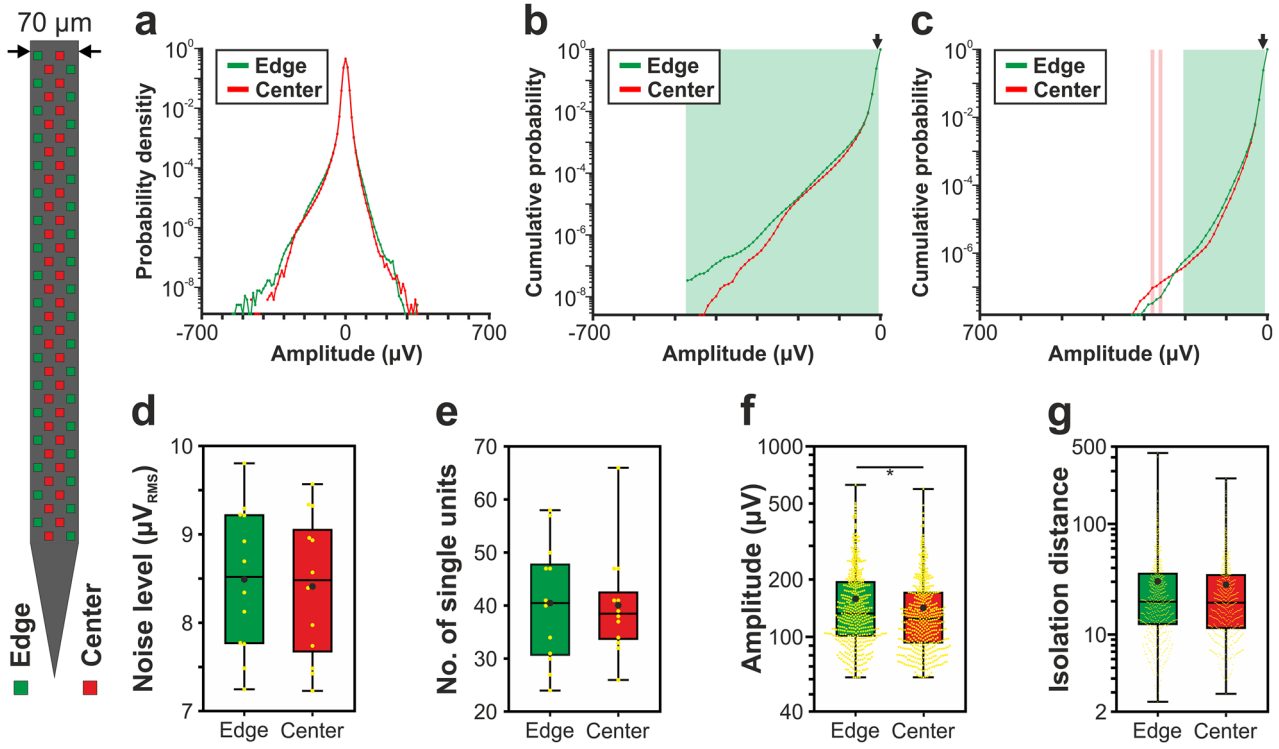

Figure 4. Comparison of the signal quality provided by edge (green) and center (red) sites of the 70-µm-wide Neuropixels silicon probe. (**a**) Probability density functions estimated from the amplitude of samples recorded in the 500–5000 Hz frequency range (n = 6 recordings). Probability values lower than 10^{-9} are not shown. (**b**) Cumulative distributions of amplitudes calculated in the negative amplitude range. (**c**) Reverse cumulative distributions calculated in the positive amplitude range. Green (or red) shaded areas in (**b**) and (**c**) indicate amplitudes with significantly higher numbers of edge (or center) samples. Arrows mark the maximal amplitude for edge significance in the negative range (− 10 µV; below this amplitude 12.20% of all negative samples were recorded on edge sites and 12.14% on center sites) and the minimal amplitude in the positive range (10 µV; above this amplitude 12.21% of all positive samples were recorded on edge sites and 12.15% on center sites). (**d**) Estimated in vivo noise level. (**e**) Single unit yield (n = 967). (**f**) Peak-to-peak amplitude of the averaged single unit spike waveforms. (**g**) Isolation distance of the single unit clusters. Note that most data are plotted on a logarithmic scale. Mann–Whitney *U* test was used in (**d**–**g**). *p < 0.05.

Spike sorting and calculation of single unit properties. To assign the recorded spikes to individual neurons, automatic spike sorting was performed on recordings separated by site position using the MATLAB-based software Kilosort[58]. Manual revision of the single unit clusters detected by Kilosort was done in Phy, an open source neurophysiological data analysis package written in Python (github.com/kwikteam/phy). The manual revision was done blindly, that is, the user did not know whether the actual data file was recorded by edge or center sites. After the revision of spike sorting results, wideband spikes of each single unit cluster were averaged together to obtain the average spike waveforms. For further analysis, we selected well-isolated units using the following criteria[27]. We defined a single unit as well isolated if it had a clear refractory period (less than 2% of the spikes in the 2-ms-long refractory period), a firing rate higher than 0.05 Hz (or at least 100 spikes in the cluster) and a spike waveform with a peak-to-peak amplitude over 60 µV. The peak-to-peak amplitude was defined as the amplitude difference between the negative peak (or trough) and the largest positive peak of the average spike waveform, computed on the recording channel which contained the spikes of the particular single unit with the highest amplitude. These criteria allowed us to exclude low quality units as well as to decrease the effect of subjective decisions of the operator during the manual curation of neuron clusters. Only a low percent of the units was excluded from the analysis (from 1 to 12%; Supplementary Table 7). The following single unit properties were calculated and used to compare the signal quality of edge and center sites: single unit yield, peak-to-peak amplitude of the average spike waveform of each well-separated single unit, and the isolation distance of each unit cluster[59] (github.com/cortex-lab/sortingQuality). It is important to note that, because the silicon probes contain closely packed recording sites (with interelectrode distances ranging from 6 to 50 µm), in the case of edge and center recordings which were obtained from the same recording position, there will be some redundancy among the sorted single units. For example, a large amplitude unit detected in a recording containing only edge sites might also be detected and sorted, with a smaller spike amplitude, in the recording comprising the adjacent center sites. However, to simulate probes that contain only edge or center sites and to compare their recording performance, we wanted to treat units on adjacent site positions independently. The total unit yield of the separated recordings will be about two times higher compared to the unit yield obtained by sorting the original recordings with all channels included (Supplementary Table 8).

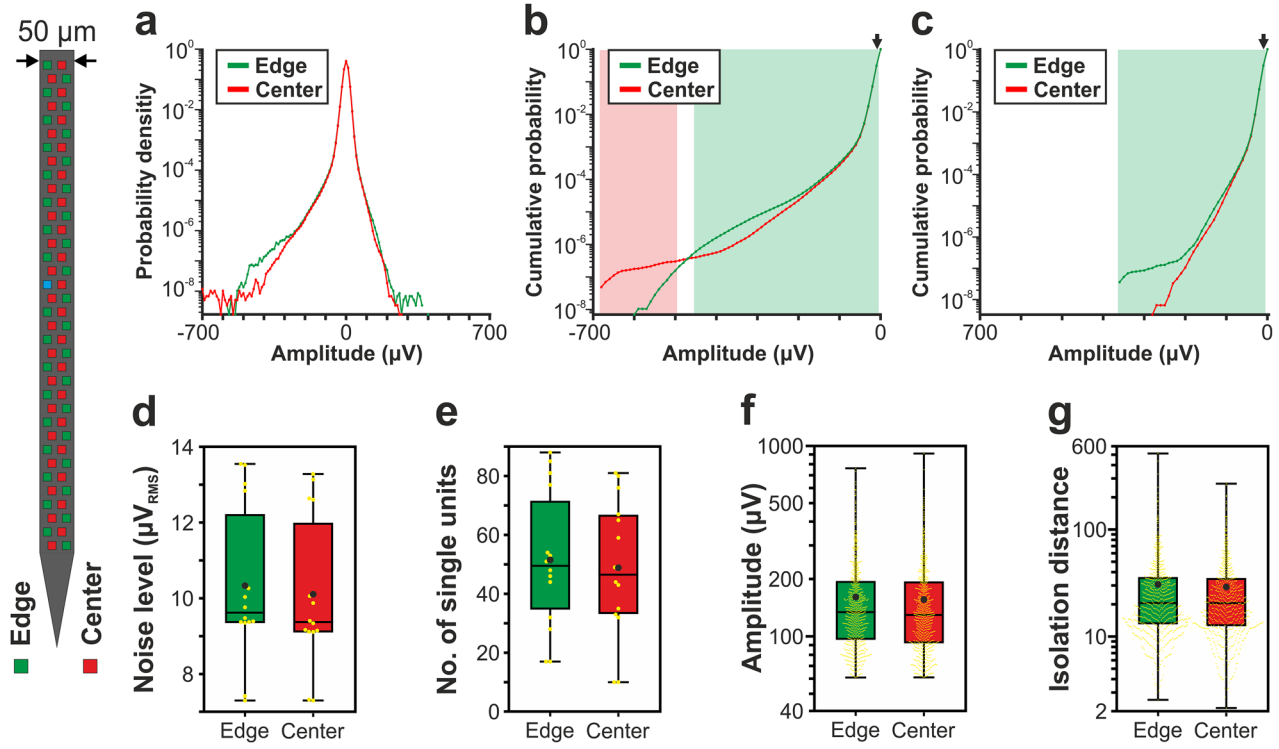

Figure 5. Comparison of the signal quality provided by edge (green) and center (red) sites of the 50-µm-wide Neuropixels silicon probe. (**a**) Probability density functions estimated from the amplitude of samples recorded in the 500–5000 Hz frequency range (n = 7 recordings). Probability values lower than 10^{-9} are not shown. (**b**) Cumulative distributions of amplitudes calculated in the negative amplitude range. (**c**) Reverse cumulative distributions calculated in the positive amplitude range. Green (or red) shaded areas in (**b**) and (**c**) indicate amplitudes with significantly higher numbers of edge (or center) samples. Arrows mark the maximal amplitude for edge significance in the negative range (− 10 µV; below this amplitude 15.73% of all negative samples were recorded on edge sites and 15.57% on center sites) and the minimal amplitude in the positive range (10 µV; above this amplitude 15.20% of all positive samples were recorded on edge sites and 15.03% on center sites). (**d**) Estimated in vivo noise level. (**e**) Single unit yield (n = 1405). (**f**) Peak-to-peak amplitude of the averaged single unit spike waveforms. (**g**) Isolation distance of the single unit clusters. Note that most data are plotted on a logarithmic scale. Mann–Whitney *U* test was used in (**d**–**g**).

Estimation of the noise level of the filtered signal in vivo. Although it would be possible to measure the noise level of recording sites using data obtained in vitro in saline solution, we did not have access to all probe types to perform these tests. Therefore, we developed a method to estimate the noise level based on in vivo recordings. Because most cortical neurons cease to fire for a couple of hundred milliseconds during down-states of the ketamine-xylazine or urethane-induced slow wave activity[57], the signals recorded during these short time windows of neuronal silence might be appropriate to approximate the noise level of recordings. We used a state detection algorithm previously developed by our group[57] to detect the onset of up- (high spiking activity) and down-states (low spiking activity; Supplementary Fig. 3). First, the wideband signal was filtered (500–5000 Hz; Butterworth 3rd-order bandpass filter; zero-phase shift) and rectified to extract the multiunit activity (MUA). After that, all channels were summed up sample-wise (Summed MUA; Supplementary Fig. 3) then smoothed using a 50 Hz lowpass filter to extract the envelope of the MUA (Smoothed MUA; Supplementary Fig. 3). Next, using a threshold level (calculated by also taking into account the duration of slow wave states), we detected the state onsets. Finally, on each channel of the rectified MUA, the root mean square (RMS) value of a 50-ms-long segment in the middle of down-states with a duration of at least 200 ms was calculated, then the RMS values were averaged (Supplementary Fig. 3). The method was validated by in vitro measurements of the RMS noise of recording sites of 128-channel and 255-channel probes in saline solution. For the 128-channel probe (n = 6 probes), the estimated noise level in the 500–5000 Hz frequency range was around 80% higher than the noise level measured in vitro (in vivo vs. in vitro: 3.87 ± 0.43 μV_{RMS} vs. 2.17 ± 0.66 μV_{RMS}; mean ± standard deviation). For the 255-channel probe (n = 2 probes), this difference was about 65% (in vivo vs. in vitro: 6.87 ± 0.41 μV_{RMS} vs. 4.15 ± 0.58 μV_{RMS}). A similar difference was also found in the case of the Neuropixels probes (10.22 ± 2.01 μV_{RMS} for the 50 µm wide probe and 8.45 ± 0.81 μV_{RMS} for the 70 µm wide probe vs. 5.1 ± 0.6 μV_{RMS} reported in vitro in Ref.[3]). Thus, although our method slightly overestimates the noise level, it is suitable to measure this property and compare it between edge and center sites.

Statistical analysis. To test the difference between the mean signal power of center and edge sites, Brown-Forsythe test for equal variances was applied. The Brown-Forsythe statistics follows F-distribution, and it is less

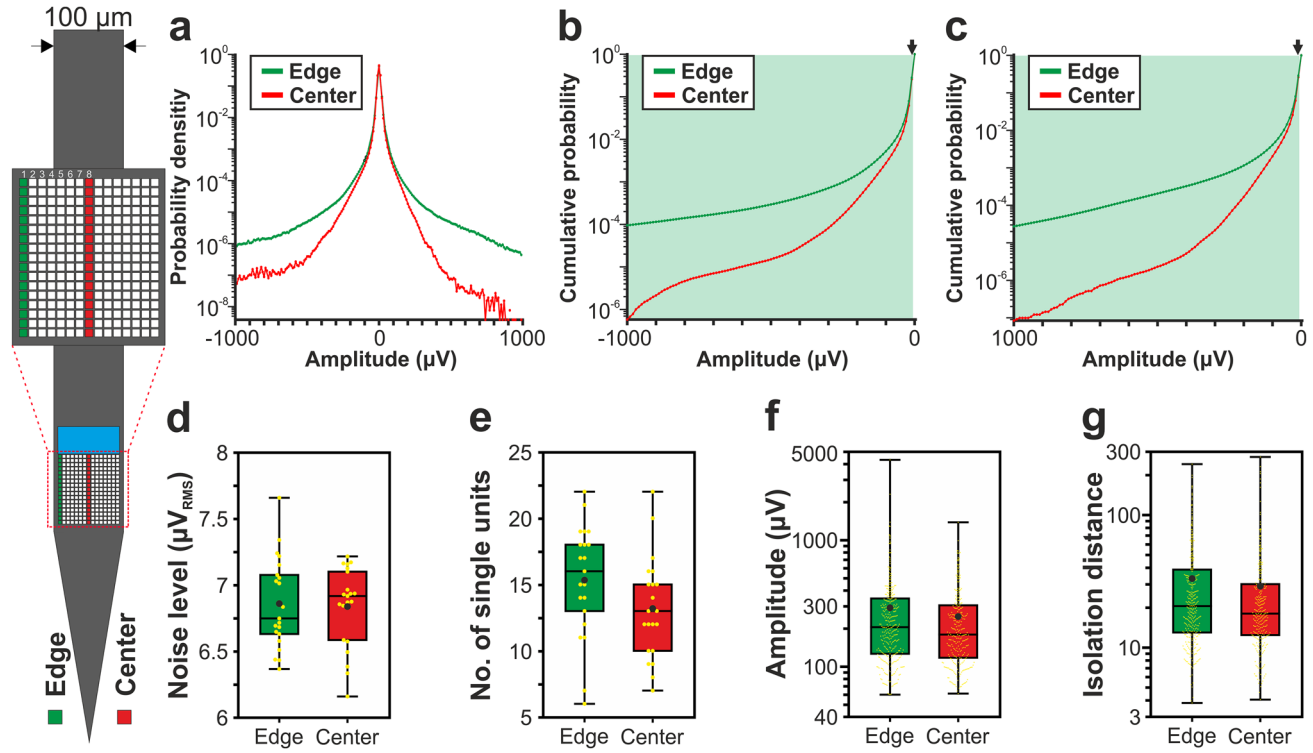

Figure 6. Comparison of the signal quality provided by edge (green) and center (red) sites of the 255-channel NeuroSeeker silicon probe. (**a**) Probability density functions estimated from the amplitude of samples recorded in the 500–5000 Hz frequency range (n = 21 recordings). Probability values lower than 10^{-9} are not shown. (**b**) Cumulative distributions of amplitudes calculated in the negative amplitude range. (**c**) Reverse cumulative distributions calculated in the positive amplitude range. Green shaded areas in (**b**) and (**c**) indicate amplitudes with significantly higher numbers of edge samples. Arrows mark the maximal amplitude for edge significance in the negative range (− 10 µV; below this amplitude 14.45% of all negative samples were recorded on edge sites and 12.57% on center sites) and the minimal amplitude in the positive range (10 µV; above this amplitude 14.82% of all positive samples were recorded on edge sites and 12.63% on center sites). (**d**) Estimated in vivo noise level. (**e**) Single unit yield (n = 599). (**f**) Peak-to-peak amplitude of the averaged single unit spike waveforms. (**g**) Isolation distance of the single unit clusters. Note that most data are plotted on a logarithmic scale. Mann–Whitney *U* test was used in (**d**–**g**).

sensitive to the non-normal distribution of the samples than the F-statistic. The statistical analysis regarding the binomial distributions is described in the "Amplitude distribution of the filtered potential" section.

Because the variables noise level, single unit yield, spike amplitude and isolation distance had a low sample size or non-normal distribution (according to the Kolmogorov–Smirnov and Shapiro–Wilk tests) we used non-parametric tests for statistical analysis (Supplementary Table 9). Mann–Whitney *U* test was applied to compare the performance of edge and center sites (two groups, Figs. 2, 3, 4, 5 and 6), while Kruskal–Wallis test was used for the comparison of laterality (three or four groups, Supplementary Figs. 9–12 and Supplementary Fig. 14). When a significant difference was found between site positions by the Kruskal–Wallis test, post-hoc analysis was performed for all pairwise comparisons using Dunn's test with Bonferroni correction. p values less than 0.05 were considered significant. Effect sizes were calculated using the following formula: $r = Z/\sqrt{N}$, where Z is the z-score and N is the sample size. Features of boxplots (Figs. 2, 3, 4, 5 and 6; Supplementary Figs. 9–12 and Supplementary Fig. 14) showing the distribution of data are presented as follows. The middle line indicates the median, while the boxes correspond to the 25th and 75th percentile. Whiskers mark the minimum and maximum values. The average is depicted with a black dot, whereas individual values are indicated with smaller yellow dots.

Results

To examine whether there is a difference in the recording performance of edge and center sites, we analyzed recordings obtained with commercially available and state-of-the-art high-density silicon probes with channel numbers ranging from 32 to 384 (NeuroNexus, Neuropixels and NeuroSeeker probes; Fig. 1; see "Silicon probe types" in the Methods section for details). These single-shank planar probes contain recording sites both in the center and close to the edge of their silicon shank which makes them suitable to assess and compare the neural signal quality at these site positions. Furthermore, the different probe widths (from 50 to 125 µm) allow us to investigate width-dependent effects of the recording capability of edge and center sites. Quantitative details of in vivo experiments and cortical recordings are summarized in Table 1.

To compare the signal quality provided by edge and center sites, we first separated channels of the spontaneous cortical recordings based on their site locations (Supplementary Fig. 2; see "Grouping of recording sites" in

	32-channel NN probe		128-channel NS probe		70 µm wide NP probe		50 µm wide NP probe		255-channel NS probe	
	Edge	Center	Edge	Center	Edge	Center	Edge	Center	Edge	Center
RMS of amplitudes	12.26	11.96	11.69	11.19	9.67	9.53	10.99	10.86	23.67	14.08
No. of single units	14.95 ± 3.73	13.10 ± 2.28	26.15 ± 4.44	26.45 ± 5.02	40.50 ± 11.49	40.08 ± 10.16	51.50 ± 23.85	48.86 ± 23.60	15.33 ± 4.23	13.19 ± 3.82
Amplitude of single units (µV)	226.04 ± 117.56	220.11 ± 97.39	184.94 ± 102.10	164.65 ± 85.37	157.19 ± 82.85	140.93 ± 70.14	159.71 ± 95.88	154.97 ± 92.76	292.45 ± 334.63	249.39 ± 191.66
Isolation distance	24.38 ± 23.86	21.35 ± 17.30	37.08 ± 42.14	33.52 ± 38.56	30.25 ± 37.02	28.25 ± 29.85	30.71 ± 37.73	29.04 ± 28.95	33.20 ± 34.66	29.08 ± 35.14
Noise level (μV_{RMS})	5.72 ± 0.79	5.87 ± 0.75	3.88 ± 0.42	3.86 ± 0.44	8.49 ± 0.82	8.41 ± 0.83	10.34 ± 2.09	10.11 ± 2.01	6.88 ± 0.45	6.84 ± 0.30

Table 2. Mean ± standard deviation of the calculated features for all probe types (NN, NeuroNexus; NS, NeuroSeeker; NP, Neuropixels). The root mean square (RMS) of amplitudes was calculated by pooling samples of all recordings.

	32-channel NN probe		128-channel NS probe		70 µm NP probe		50 µm NP probe		255-channel NS probe	
	p-value	effect size	p-value	effect size	p-value	effect size	p-value	effect size	p-value	effect size
Amplitude distributions	**< 0.001**		**< 0.001**		**< 0.001**		**< 0.001**		**< 0.001**	
No. of single units	0.17	0.25	0.935	-0.013	0.885	0.03	0.696	0.074	0.064	0.286
Amplitude of single units (µV)	0.812	0.011	**0.001**	0.104	**0.002**	0.1	0.226	0.032	0.105	0.066
Isolation distance	0.687	0.019	0.122	0.048	0.479	0.023	0.477	0.019	0.057	0.078
Noise level (μV_{RMS})	0.328	-0.185	0.766	0.047	0.862	0.035	0.383	0.165	0.99	0.002

Table 3. Summary of statistical analysis. Brown-Forsythe test was applied to compare the amplitude distributions, while Mann–Whitney U test was used in the case of the last four features. Significant ($p < 0.05$) values are indicated in bold (NN, NeuroNexus; NS, NeuroSeeker; NP, Neuropixels).

the Methods section for details), then extracted multiple features from the signals, focusing on the 500–5000 Hz frequency range corresponding to single unit activity. The amplitude of extracellular spikes quickly decays with distance[1,60], that is, neurons located closer to recording sites will produce larger spikes which usually provides a better separability from spikes of other neurons. Thus, measures related to spike amplitude might be suitable to compare the quality of edge and center recordings. In addition, a higher proportion of high-amplitude spikes in the data might indirectly reflect a tissue damage of smaller extent, that is, the presence of more neurons which survived the probe insertion and were located close to a particular site[27]. Here, we examined the amplitude distribution of the filtered potential recorded at different site positions in the range from − 1000 to 1000 µV (see "Amplitude distribution of the filtered potential" in the Methods section for more details). To ascertain that differences in the amplitude distributions are not biased by differences in noise level between edge and center sites, we estimated the level of noise in the analyzed recordings based on the in vivo data (Supplementary Fig. 3; see "Estimation of the noise level of the filtered signal in vivo" in the Methods section for more details). In addition, spike sorting was performed on the recordings to extract the following single unit properties for comparison: single unit yield, amplitude of single unit spikes and isolation distance (see "Spike sorting and calculation of single unit properties" in the Methods section for more details). The latter is a measure commonly used to determine the quality of single unit clusters[59], while the former are usual features used to assess the recording performance extracted under different conditions[27,61]. The unit yield as well as properties corresponding to the quality of single units (spike amplitude, isolation distance) are important measures that can demonstrate the practical usability of probes in electrophysiological experiments. Thus, albeit the extraction of these features is more time-consuming compared to the analysis of the amplitude distribution, these might give us a more detailed picture of the recording performance of different site positions. Example recordings and single unit spike waveforms obtained with each probe type at different site positions are shown in Supplementary Figs. 4–8. Since the results were similar for the left and right sides of the probes, for each site position, we pooled the data corresponding to the two sides and did the analysis on the combined data (Figs. 2, 3, 4, 5 and 6; Tables 2, 3, 4, and 5). However, data of both sides can be found separately in the Supplementary Material (panels a–e of Supplementary Figs. 9–12; Supplementary Tables 3, 4, 5 and 6).

Comparison of the amplitude distribution of the filtered potential between different site positions. Results corresponding to the analysis of the amplitude distributions are demonstrated in panels a–c of Figs. 2, 3, 4, 5 and 6, while the root mean square (RMS) values indicating the total power of these distributions, as well as the results of statistical analyses, are summarized in Tables 2 and 3, respectively. The noise level of recordings was low with a low variance across recordings, and there was no statistically significant difference in the noise level of edge and center sites for either probe type (panel d of Figs. 2, 3, 4, 5 and 6; Tables 2 and

Probe type	Negative amplitude threshold (μV)	% of negative samples on edge sites	% of negative samples on center sites
NeuroNexus 32-channel probe	− 20	2.95	2.93
NeuroSeeker 128-channel probe	− 10	8.70	8.64
Neuropixels probe (70 μm wide)	− 10	12.20	12.14
Neuropixels probe (50 μm wide)	− 10	15.73	15.57
NeuroSeeker 255-channel probe	− 10	14.45	12.57

Table 4. Maximal negative amplitude thresholds below which significantly more edge samples were detected.

Probe type	Positive amplitude threshold (μV)	% of positive samples on edge sites	% of positive samples on center sites
NeuroNexus 32-channel probe	40	0.59	0.57
NeuroSeeker 128-channel probe	10	9.02	8.92
Neuropixels probe (70 μm wide)	10	12.21	12.15
Neuropixels probe (50 μm wide)	10	15.20	15.03
NeuroSeeker 255-channel probe	10	14.82	12.63

Table 5. Minimal positive amplitude thresholds above which significantly more edge samples were detected.

3). Examining the distribution of sample amplitudes (panel a of Figs. 2, 3, 4, 5 and 6) showed that in almost all cases edge sites provided a higher signal quality (shown by higher probability values) which was also indicated by higher RMS values (Table 2). The difference between edge and center amplitude distributions was significant for each probe type (Table 3). The statistical analysis of the cumulative amplitude distributions allowed us to determine the negative (positive) amplitudes below (above) which significantly more edge or center samples were recorded (Figs. 2, 3, 4, 5 and 6b,c; Tables 4 and 5). In most cases, the results indicated significantly more samples on edge sites below − 10 μV in the negative amplitude range (Figs. 2, 3, 4, 5 and 6b; Table 4) and above 10 μV in the positive amplitude range (Figs. 2, 3, 4, 5 and 6c; Table 5). In the negative amplitude range, based on the ratio of the probability density values of edge sites to center sites, the difference between site positions was most remarkable in the range corresponding to the largest spikes (below − 250 μV; Fig. 7a) but the difference in the sample numbers of edge and center sites is still clearly visible until about − 50 μV.

To examine whether there might be shank width-dependent differences in the recording performance between edge and center sites, for each probe type, we averaged the ratio of edge-to-center values demonstrated in panel a of Fig. 7 over the whole amplitude range. Our results show, that with decreasing shank width, a slightly decreasing trend in these averages can be observed (Fig. 7b). This suggests that the performance advantage of edge sites becomes smaller for narrower probes.

By investigating recordings obtained with the 255-channel probe providing a superior spatial resolution (Fig. 6), we can perform a finer and more detailed analysis to compare the recording performance of sites located at different distances from the edge of the silicon shank. Therefore, we analyzed the amplitude distribution of recordings obtained at eight adjacent columns of recording sites (17 sites in each column) located on the left side of probe (Supplementary Fig. 13; Supplementary Table 10). The highest RMS value was provided by the first column of sites (located at the edge), whereas the lowest RMS value was measured at the recording sites located in the center of the shank (Supplementary Table 10), showing a slightly decreasing trend towards the center of the silicon shank. This trend can also be observed in the figure showing the probability distributions of amplitudes recorded by various site columns (Supplementary Fig. 13).

To further investigate the robustness of our results, we analyzed a public dataset (n = 7 cortical recordings) obtained with the same type of 255-channel probe as used in this study (Supplementary Fig. 14a; Supplementary Table 11). Again, RMS values corresponding to edge sites were higher compared to the RMS value of center sites. Interestingly, however, based on the cumulative distributions, center sites performed slightly better in the range containing the largest spikes. This difference might probably be caused by differences in the anesthesia, insertion conditions, the targeted brain region or the number of recordings used for analysis (i.e., the sample size). Nevertheless, the overall signal quality was still somewhat better at edge sites than at center sites.

To examine the influence of sample size on the obtained results, we analyzed a larger dataset (n = 179 cortical recordings) acquired with the 128-channel NeuroSeeker probe (Supplementary Fig. 15; Supplementary Tables 12–13). Although the RMS values were lower compared to the values presented in Table 2 (because the larger dataset also contained recordings which were acquired from cortical layers with lower neuronal activity, for example, from layers I–III), differences between the amplitude distributions of edge and center sites were still significant.

The neocortex has a special anatomical structure with multiple layers, areas, columns and various cell types[62]. To examine whether there might by brain area-dependent differences in the recording performance of edge and center sites, we analyzed recordings (n = 9) from the somatosensory thalamus obtained with the 128-channel probe (Supplementary Fig. 16; Supplementary Tables 14 and 15). Again, edge sites provided better signal quality compared to center sites in the investigated amplitude range, although the difference in recording performance was smaller.

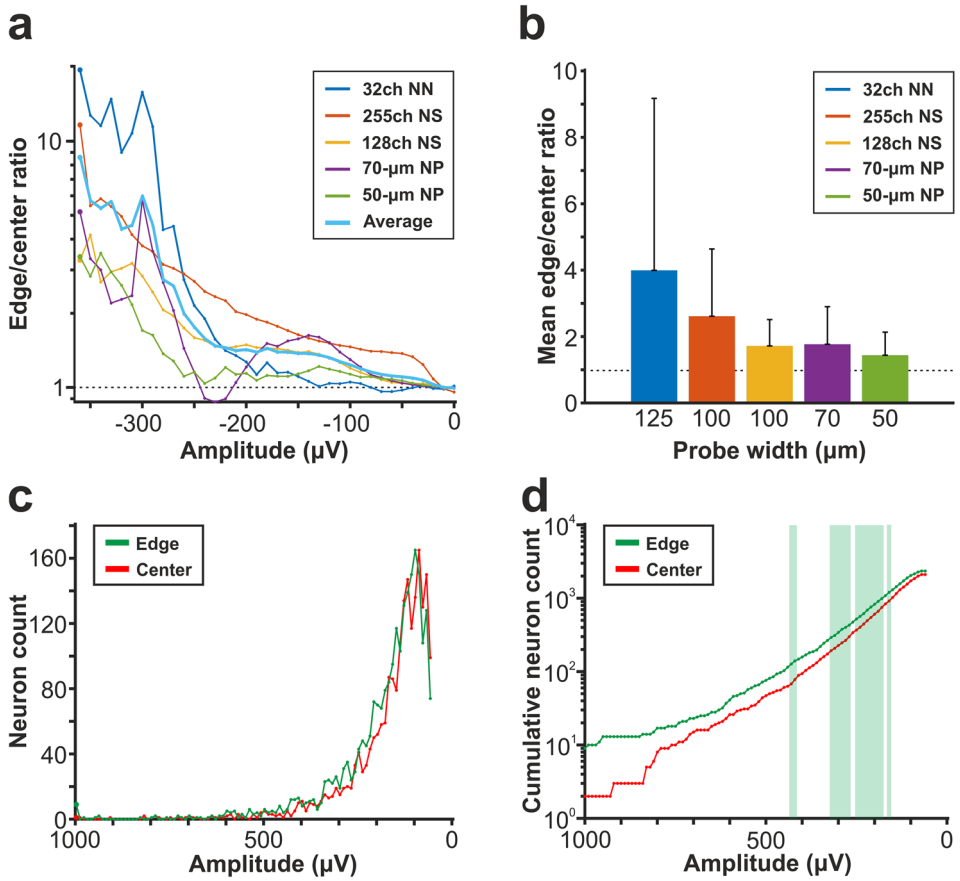

Figure 7. Summary of the recording performance comparison of edge and center sites. (**a**) Ratio of the probability density values of edge sites to center sites calculated in the negative amplitude range from 0 μV to − 1000 μV, for each probe type. The larger first dot represents the sum of the probability values computed in the range below − 350 μV. The dashed line indicates the position where the probability of edge samples and center samples is equal. The thick line with light blue color shows the average of the five probes. (**b**) Values illustrated in (**a**) averaged over the whole negative amplitude range for each probe type (mean ± standard deviation). Probes are ordered by shank width. (**c**) Distributions of the spike amplitudes of all single units recorded on edge (green, n = 2351 units) and center (red, n = 2102 units) sites. Note that the direction of the x-axis is reversed. (**d**) Reverse cumulative distributions of spike amplitudes calculated from (**c**). Green shaded areas indicate amplitudes with significantly higher numbers of edge units. In (**c**) and (**d**), amplitudes start at 60 μV.

It would be interesting to examine whether there are differences in the recording performance between sites located at different longitudinal positions of the silicon shank. To investigate that, we analyzed the same cortical (n = 10) and thalamic (n = 9) recordings obtained with the 128-channel silicon probes (Supplementary Fig. 17; Supplementary Tables 16 and 17). However, instead of edge/center grouping, four site groups (32 channels in each group) were created based on their vertical locations (Supplementary Fig. 17a). For recordings from both brain structures, the RMS values and amplitude distributions showed that the site group located in the lower middle of the shank (second group of 32-channels, calculated from the bottom) provided the best recording performance (Supplementary Fig. 17b,c; Supplementary Tables 16 and 17). However, the results might be slightly biased in the case of cortical recordings, since the intensity of spiking activity significantly varies across cortical layers in ketamine/xylazine anesthetized rats[57] (Supplementary Fig. 17d). Unit activity was found to be the strongest in the lower part of layer V (which has a thickness of about 300 μm), and is weaker in upper and lower layers[57]. Because recordings with the 128-channel probe were acquired from multiple cortical layers simultaneously (usually layers IV–VI), the layer-dependent intensity of spiking activity might affect our results obtained here. Results obtained with thalamic recordings might provide a more accurate comparison because the recorded spiking activity was more uniform at different dorsoventral depths compared to cortical activity (Supplementary Fig. 17d). Although small differences in the structure of the examined thalamic area, or depth-dependent differences in thalamic activity (e.g. by recording simultaneously from multiple thalamic nuclei), may still slightly decrease the reliability of these findings.

In summary, edge sites provided a higher performance compared to center sites for all probe types. Such differences in signal quality could be observed in different brain areas, and also at different longitudinal positions of the recording sites. The better performance of the edge sites decreased with decreasing shank width.

Comparison of single unit properties between edge and center sites. Boxplots corresponding to the analysis of single units are demonstrated in panels e–g of Figs. 2, 3, 4, 5 and 6, while mean values and the results of statistical analyses are summarized in Tables 2 and 3, respectively. In almost all cases, edge sites provided a higher signal quality which was indicated by higher mean values of the single unit yield, spike amplitude and isolation distance (Table 2). The average number of well-separated single units recorded at a particular cortical location ranged from ~ 15 (32-channel NeuroNexus and 255-channel NeuroSeeker probes) to ~ 50 (50-µm-wide Neuropixels probe). The difference in the single unit yield was small and not significant between site positions, usually only a few more units could be separated on edge sites. However, the spike amplitudes of single units obtained at edge sites of the 128-channel NeuroSeeker probe and the wider Neuropixels probe were significantly higher compared to unit amplitudes at center sites. Overall, significantly more single units having spike waveforms with peak-to-peak amplitudes over 150 µV were detected on edge sites (Fig. 7c,d). This suggests that either more neurons were located closer to edge sites than to center sites (e.g. due to tissue compression caused by the probe) or more neurons survived the mechanical trauma of probe insertion in the vicinity of edge sites.

Discussion

Our results, based on in-depth quantitative analysis of high-density neural recordings obtained with commercially available and state-of-the-art silicon probes, showed that, for all probe types examined, the recording performance of edge sites was slightly better than that of center sites. Examined features of the filtered signal containing spiking activity had in most cases higher values for edge sites. Differences between the two site positions were also significant in several cases, and these differences indicated in almost every case a better signal quality recorded on edge sites. These differences were most remarkable in the amplitude range corresponding to large spikes (with a negative peak smaller than – 250 µV; Fig. 7a). Furthermore, we have found that the shank width of the probe might also affect the difference in recording performance: edge sites lose their advantage with narrower shanks (Fig. 7b). Although the single unit yield was not significantly higher between site positions, on average, the amplitude of the unit spike waveforms was usually larger, and the quality of unit clusters was better for edge sites (Fig. 7c,d). The small difference in the single unit yield and the small effect sizes found in the case of single unit features might suggest only a moderate practical applicability of our findings; however, the significantly larger spikes recorded at edge sites suggest that edge recordings may slightly improve the separability of single unit clusters, and thus the accuracy and reliability of spike sorting results.

Out of three studies investigating the recording performance of microelectrodes located on the edge and the center of probe shanks[34–36], the results of two studies are in agreement with our findings, that is, placing recording sites on the edge improves the quality of the recorded neural signal. Lee and colleagues chronically implanted custom-designed 16-channel silicon probes with two different widths into the motor cortex of rats to track their recording performance for several weeks[35]. Seven and eight quadratic recording sites (30 µm × 30 µm) were placed in the center and at the edge of the probe shank, respectively. Compared to center sites, the chronic recording capability of edge sites of the wider probe was significantly better for several weeks in terms of the ratio of sites containing spiking activity as well as the signal-to-noise ratio of separated single units. Although the results were not significant, edge sites of the planar silicon probe with the narrower shank (132 µm) still performed better than center sites. Our comprehensive study extended these results by analyzing data obtained with probes having narrower shanks (from 50 to 125 µm). Interestingly, edge sites still provided better recordings even with the narrowest device, although the advantage of edge sites decreased notably with decreasing shank widths.

The custom-designed probes developed by Seymour and colleagues[36] had microelectrodes fabricated in the lateral wall of the parylene shank (edge sites) in combination with recording sites placed on the front and back side of the shank located further from the shank edge. They could separate more single units in recordings obtained with edge sites and the measured spike amplitudes were also higher. Although we found no difference in the single unit yield between edge and center sites, edge sites on the investigated high-density probes are located not exactly on the edge but a few micrometers towards the center. In contrast, the special edge design used in Ref. 36 might provide a better accessibility to neurons and a wider viewing angle to detect their action potentials due to a decreased shielding effect of the probe shank[63,64].

In the work of Scott et al.[34], an 85 µm wide single-shank silicon probe with 64 recording sites arranged in three columns (two on each side and one in the center of the shank) was used to record spiking activity from the hippocampus of mice. They found no difference in the signal quality between edge and center sites, as well as between spike amplitudes measured on sites located at different longitudinal positions of the shank. The discrepancy between their results and our findings might be caused by several factors such as the difference in animal species, the examined brain area or the used methodology.

As described above, recording sites classified as edge sites in this study are located slightly further (~ 5–6 µm) from the edge of the silicon shank. Thus, our results obtained with edge sites might slightly underestimate the real recording performance of microelectrodes placed exactly at the edge of the shank, for example, in the case of special edge probe designs[36,41,65] which provide an even larger field of view for signal detection.

The focus of this study was on the analysis of cortical recordings. However, as demonstrated by comparing the performance of edge and center sites between thalamic and cortical recordings (with a larger difference in the signal quality in the neocortex), the performance advantage of edge sites might also depend on the anatomical structure, cellular density and composition of the examined brain region. This theory is further supported

by the findings of the study of Scott and colleagues, where no difference was found in the recording capabilities of edge and center sites in another brain region, namely in the hippocampus of mice[34]. In contrast, in the case of the two studies which have found a difference in the signal quality between edge and center sites, the probes were implanted into the motor cortex of rats[35,36]. Therefore, testing the recording performance of edge and center sites in other brain areas as well as in other species might further our knowledge of optimal site placement on silicon probes.

Other factors might also influence the quality of recordings, and thus might affect the performance difference between edge and center sites. For instance, a computational modeling study demonstrated that both edema and glial encapsulation can have a significant impact on the amplitude of the recorded spikes, with a decrease of amplitude in the former case and an increase in the latter case[63]. Thus, a localized edema developed due to a minor tissue damage near the edge of the shank might diminish the performance advantage of affected edge sites. Moreover, a glial scar formed around chronically implanted silicon probes might be more pronounced close to the sharp edges of the probe where small micromotions of the implant mechanically insult the tissue[66,67]. This difference in glial density or thickness might influence the signal quality of recording sites, especially those located at the edges. Although we only analyzed recordings of acute experiments with a relatively short duration (~ 30 min), results of the work of Lee et al.[35] suggest that edge sites might keep their performance advantage over center sites also over longer timescales, even for several weeks.

The speed of probe insertion may also significantly affect recording quality[27]. Analyzing the dataset of our previous study[27], we found that, in acute recordings, the performance difference between edge and center sites was larger when slower speeds (< 0.1 mm/s) were used for insertion (data not shown). As the speed of insertion affects the extent of neuronal loss around the probe[27], this suggests that using a higher insertion speed will result in more severe tissue damage close to the edges of the probe.

Based on our current knowledge, we can only speculate on the causes behind the observed differences in recording performance of edge and center sites. One plausible explanation might be that edge sites have a better "visibility" compared to center sites, that is, they are less affected by the shielding or shadowing effect of the silicon or parylene substrate[36,63]. Therefore, microelectrodes located closer to the edge of the shank should detect the action potentials of more neurons. However, we did not find a higher single unit yield for edge sites. The main difference in the recording performance between the two site positions was in the amplitude of spikes, mostly in high amplitude ranges corresponding to the largest spikes. Because the spike amplitude rapidly attenuates with increasing distance from the soma of the neuron[1,60], higher spike amplitudes on edge sites may suggest that several neurons are located closer to edge sites than to center sites. The reason behind this asymmetry in the distance of neurons might be that more neurons survive the implantation of the probe which are close to the edge of the shank compared to cells located close to the center. However, this scenario should probably also result in a higher unit yield for edge sites. Another possible explanation might be that, since the width of these probes is larger than their thickness, the tissue compression caused by the probe is asymmetric and is higher along the lateral axis than along the axis corresponding to the front and backside of the probe. Thus, neurons might be slightly more compressed near edge sites and pushed closer to them. Therefore, using a probe shank with a smaller cross-section should result in the decrease of performance difference between the two site positions, as the degree of tissue compression will be smaller. We could observe this decrease in performance: although still present, the advantage of edge site over center sites slightly decreased with decreasing shank width.

It is also important to mention, that the shielding effect of the probe shank may also affect the recorded spike amplitudes[36,46,63]. One computational modeling study showed that when a modeled probe shank is placed before the model neuron, the recorded spike amplitudes are almost two times higher compared to the amplitude of simulated spikes obtained without the presence of the probe shank[63]. In a recent modeling study, using mesh models of NeuroNexus and Neuropixels probes, Buccino and colleagues demonstrated similar findings, that is, the use of silicon probes significantly amplified the recorded potentials[46]. They have also found that almost two times higher action potential amplitudes can be detected when the probe shank is present. This difference in the spike amplitudes decreased when the model neuron was shifted from the center of the shank laterally to the edge. For instance, in the case a 50 µm lateral shift, the simulated spike amplitudes were only 40% higher with the probe shank included in the simulations. The authors argue that this bias might results in more neurons found in the probe center than at the edges. If the shielding of the probe substrate has a similar effect in vivo (i.e. spike amplitudes are amplified more in the probe center than at the edge), then, based on our results (i.e. higher spike amplitudes found at the edge), the effects of other factors contributing to the performance increase of edge sites compared to center sites are significantly stronger than the shielding effect of the probe shank.

Silicon microprobes are extensively used in a many electrophysiology labs. Further advancements in probe design and in silicon microfabrication technology will soon make it possible for research groups to design their own recording devices with features customized to the actual research task. This process is further facilitated by recently shared open source probe designs and open source hardware for electrophysiological experiments[37,40]. Our results might help engineers and scientists working in the field of neuroscience to determine the optimal placement of microelectrodes on the shank of planar silicon probes. For instance, placing recording sites on the edge of the shank of passive probes (which have a limited site number) may significantly enhance their recording performance. This can save time needed to perform experiments and also reduce the costs of these studies. From another aspect, our findings suggest that in the case of high-density probes with a small shank cross-section (e.g. the Neuropixels probe), where the entire shank is covered with recording sites, both edge and center sites will sample the neuronal activity with similar quality and recordings will not be biased towards either of these site positions.

Data availability

The datasets generated during and/or analyzed during the current study are available from the corresponding author on reasonable request.

Received: 30 June 2020; Accepted: 28 December 2020
Published online: 21 January 2021

References

1. Buzsáki, G. Large-scale recording of neuronal ensembles. *Nat. Neurosci.* **7**, 446–451 (2004).
2. Buzsáki, G. *et al.* Tools for probing local circuits: high-density silicon probes combined with optogenetics. *Neuron* **86**, 92–105 (2015).
3. Jun, J. J. *et al.* Fully integrated silicon probes for high-density recording of neural activity. *Nature* **551**, 232–236 (2017).
4. Raducanu, B. C. *et al.* Time multiplexed active neural probe with 1356 parallel recording sites. *Sensors* **17**, 2388 (2017).
5. Steinmetz, N. A., Koch, C., Harris, K. D. & Carandini, M. Challenges and opportunities for large-scale electrophysiology with Neuropixels probes. *Curr. Opin. Neurobiol.* **50**, 92–100 (2018).
6. Steinmetz, N. A., Zatka-Haas, P., Carandini, M. & Harris, K. D. Distributed coding of choice, action and engagement across the mouse brain. *Nature* **576**, 266–273 (2019).
7. Harris, K. D., Quiroga, R. Q., Freeman, J. & Smith, S. L. Improving data quality in neuronal population recordings. *Nat. Neurosci.* **19**, 1165–1174 (2016).
8. Márton, G. *et al.* A silicon-based microelectrode array with a microdrive for monitoring brainstem regions of freely moving rats. *J. Neural Eng.* **13**, 026025 (2016).
9. Stringer, C., Pachitariu, M., Steinmetz, N., Carandini, M. & Harris, K. D. High-dimensional geometry of population responses in visual cortex. *Nature* **571**, 361–365 (2019).
10. Stringer, C. *et al.* Spontaneous behaviors drive multidimensional, brainwide activity. *Science* **364**, 255 (2019).
11. Yang, W. & Yuste, R. In vivo imaging of neural activity. *Nat. Methods* **14**, 349–359 (2017).
12. Lin, M. Z. & Schnitzer, M. J. Genetically encoded indicators of neuronal activity. *Nat. Neurosci.* **19**, 1142–1153 (2016).
13. Weisenburger, S. & Vaziri, A. A guide to emerging technologies for large-scale and whole-brain optical imaging of neuronal activity. *Annu. Rev. Neurosci.* **41**, 431–452 (2018).
14. Fiáth, R. *et al.* A silicon-based neural probe with densely-packed low-impedance titanium nitride microelectrodes for ultrahigh-resolution in vivo recordings. *Biosens. Bioelectron.* **106**, 86–92 (2018).
15. Putzeys, J. *et al.* Neuropixels data-acquisition system: a scalable platform for parallel recording of 10,000+ electrophysiological signals. *IEEE Trans. Biomed. Circuits Syst.* **13**, 1635–1644 (2019).
16. Wang, S. *et al.* A compact quad-shank CMOS neural probe with 5,120 addressable recording sites and 384 fully differential parallel channels. *IEEE Trans. Biomed. Circuits Syst.* **13**, 1625–1634 (2019).
17. Angotzi, G. N. *et al.* SiNAPS: An implantable active pixel sensor CMOS-probe for simultaneous large-scale neural recordings. *Biosens. Bioelectron.* **126**, 355–364 (2019).
18. Herbawi, A. S. *et al.* CMOS neural probe with 1600 close-packed recording sites and 32 analog output channels. *J. Microelectromech. Syst.* **27**, 1023–1034 (2018).
19. De Dorigo, D. *et al.* Fully immersible subcortical neural probes with modular architecture and a delta-sigma ADC integrated under each electrode for parallel readout of 144 recording sites. *IEEE J. Solid-St. Circ.* **53**, 3111–3125 (2018).
20. Ruther, P. & Paul, O. New approaches for CMOS-based devices for large-scale neural recording. *Curr. Opin. Neurobiol.* **32**, 31–37 (2015).
21. Karumbaiah, L. *et al.* Relationship between intracortical electrode design and chronic recording function. *Biomaterials* **34**, 8061–8074 (2013).
22. Thelin, J. *et al.* Implant size and fixation mode strongly influence tissue reactions in the CNS. *PLoS ONE* **6**, e16267 (2011).
23. Szarowski, D. H. *et al.* Brain responses to micro-machined silicon devices. *Brain Res.* **983**, 23–35 (2003).
24. Edell, D. J., Toi, V. V., Mcneil, V. M. & Clark, L. D. Factors influencing the biocompatibility of insertable silicon microshafts in cerebral-cortex. *IEEE Trans. Biomed. Eng.* **39**, 635–643 (1992).
25. Ersen, A., Elkabes, S., Freedman, D. S. & Sahin, M. Chronic tissue response to untethered microelectrode implants in the rat brain and spinal cord. *J. Neural Eng.* **12**, 016019 (2015).
26. Biran, R., Martin, D. C. & Tresco, P. A. The brain tissue response to implanted silicon microelectrode arrays is increased when the device is tethered to the skull. *J. Biomed. Mater. Res. A* **82**, 169–178 (2007).
27. Fiáth, R. *et al.* Slow insertion of silicon probes improves the quality of acute neuronal recordings. *Sci. Rep.* **9**, 111 (2019).
28. Bjornsson, C. S. *et al.* Effects of insertion conditions on tissue strain and vascular damage during neuroprosthetic device insertion. *J. Neural Eng.* **3**, 196–207 (2006).
29. Welkenhuysen, M., Andrei, A., Ameye, L., Eberle, W. & Nuttin, B. Effect of insertion speed on tissue response and insertion mechanics of a chronically implanted silicon-based neural probe. *IEEE Trans. Biomed. Eng.* **58**, 3250–3259 (2011).
30. Neto, J. P. *et al.* Does impedance matter when recording spikes with polytrodes?. *Front. Neurosci.* **12**, 715 (2018).
31. Viswam, V., Obien, M. E. J., Franke, F., Frey, U. & Hierlemann, A. Optimal electrode size for multi-scale extracellular-potential recording from neuronal assemblies. *Front. Neurosci.* **13**, 385 (2019).
32. Cogan, S. F. Neural stimulation and recording electrodes. *Annu. Rev. Biomed. Eng.* **10**, 275–309 (2008).
33. Negi, S., Bhandari, R. & Solzbacher, F. Morphology and electrochemical properties of activated and sputtered iridium oxide films for functional electrostimulation. *J. Sens. Technol.* **02**, 138–147 (2012).
34. Scott, K. M., Du, J., Lester, H. A. & Masmanidis, S. C. Variability of acute extracellular action potential measurements with multisite silicon probes. *J. Neurosci. Methods* **211**, 22–30 (2012).
35. Lee, H. C., Gaire, J., Roysam, B. & Otto, K. J. Placing sites on the edge of planar silicon microelectrodes enhances chronic recording functionality. *IEEE Trans. Biomed. Eng.* **65**, 1245–1255 (2018).
36. Seymour, J. P., Langhals, N. B., Anderson, D. J. & Kipke, D. R. Novel multi-sided, microelectrode arrays for implantable neural applications. *Biomed. Microdevices* **13**, 441–451 (2011).
37. Siegle, J. H. *et al.* Open ephys: An open-source, plugin-based platform for multichannel electrophysiology. *J. Neural Eng.* **14**, 045003 (2017).
38. Solari, N., Sviatkó, K., Laszlovszky, T., Hegedüs, P. & Hangya, B. Open source tools for temporally controlled rodent behavior suitable for electrophysiology and optogenetic manipulations. *Front. Syst. Neurosci.* **12**, 18 (2018).
39. Nasiotis, K. *et al.* Integrated open-source software for multiscale electrophysiology. *Sci. Data* **6**, 231 (2019).
40. Yang, L., Lee, K., Villagracia, J. & Masmanidis, S. C. Open source silicon microprobes for high throughput neural recording. *J. Neural Eng.* **17**, 016036 (2020).
41. Ulyanova, A. V. *et al.* Multichannel silicon probes for awake hippocampal recordings in large animals. *Front. Neurosci.* **13**, 397 (2019).
42. Dimitriadis, G. *et al.* Why not record from every channel with a CMOS scanning probe?. *bioRxiv* **101**, 275818 (2018).

43. Neto, J. P. *et al.* Validating silicon polytrodes with paired juxtacellular recordings: Method and dataset. *J. Neurophysiol.* **116**, 892–903 (2016).
44. English, D. F. *et al.* Pyramidal cell-interneuron circuit architecture and dynamics in hippocampal networks. *Neuron* **96**, 505-520. e7 (2017).
45. Laboy-Juarez, K. J., Ahn, S. & Feldman, D. E. A normalized template matching method for improving spike detection in extracellular voltage recordings. *Sci. Rep.* **9**, 12087 (2019).
46. Buccino, A. P. *et al.* How does the presence of neural probes affect extracellular potentials?. *J. Neural Eng.* **16**, 026030 (2019).
47. Klee, J. L., Kiliaan, A. J., Lipponen, A. & Battaglia, F. P. Reduced firing rates of pyramidal cells in frontal cortex of APP/PS1 can be restored by acute treatment with levetiracetam. *bioRxiv* **1**, 739912 (2019).
48. Klein, L. *et al.* High-density electrophysiological recordings in macaque using a chronically implanted 128-channel passive silicon probe. *J. Neural Eng.* **17**, 026036 (2020).
49. Fiáth, R. *et al.* Fine-scale mapping of cortical laminar activity during sleep slow oscillations using high-density linear silicon probes. *J. Neurosci. Methods* **316**, 58–70 (2019).
50. Marques-Smith, A. *et al.* Recording from the same neuron with high-density CMOS probes and patch-clamp: A ground-truth dataset and an experiment in collaboration. *bioRxiv* **1**, 370080 (2018).
51. Sauerbrei, B. A. *et al.* Cortical pattern generation during dexterous movement is input-driven. *Nature* **577**, 386–391 (2020).
52. Musall, S., Kaufman, M. T., Juavinett, A. L., Gluf, S. & Churchland, A. K. Single-trial neural dynamics are dominated by richly varied movements. *Nat. Neurosci.* **22**, 1677–1686 (2019).
53. Luo, T. Z. *et al.* An approach for long-term, multi-probe neuropixels recordings in unrestrained rats. *bioRxiv* **1**, 039305 (2020).
54. Juavinett, A. L., Bekheet, G. & Churchland, A. K. Chronically implanted neuropixels probes enable high-yield recordings in freely moving mice. *eLife* **8**, e47188 (2019).
55. Paxinos, G. & Watson, C. *The Rat Brain in Stereotaxic Coordinates* 6th edn. (Academic Press/Elsevier, New York, 2007).
56. DiCarlo, J. J., Lane, J. W., Hsiao, S. S. & Johnson, K. O. Marking microelectrode penetrations with fluorescent dyes. *J. Neurosci. Methods* **64**, 75–81 (1996).
57. Fiáth, R. *et al.* Laminar analysis of the slow wave activity in the somatosensory cortex of anesthetized rats. *Eur. J. Neurosci.* **44**, 1935–1951 (2016).
58. Pachitariu, M., Steinmetz, N., Kadir, S., Carandini, M. & Harris, K. D. Kilosort: Realtime spike-sorting for extracellular electrophysiology with hundreds of channels. *bioRxiv* **1**, 061481 (2016).
59. Schmitzer-Torbert, N., Jackson, J., Henze, D., Harris, K. & Redish, A. D. Quantitative measures of cluster quality for use in extracellular recordings. *Neuroscience* **131**, 1–11 (2005).
60. Gold, C., Henze, D. A., Koch, C. & Buzsaki, G. On the origin of the extracellular action potential waveform: A modeling study. *J. Neurophysiol.* **95**, 3113–3128 (2006).
61. Fiáth, R. *et al.* Long-term recording performance and biocompatibility of chronically implanted cylindrically-shaped, polymer-based neural interfaces. *Biomed. Technol.* **63**, 301–315 (2018).
62. Harris, K. D. & Shepherd, G. M. The neocortical circuit: Themes and variations. *Nat. Neurosci.* **18**, 170–181 (2015).
63. Moffitt, M. A. & McIntyre, C. C. Model-based analysis of cortical recording with silicon microelectrodes. *Clin. Neurophysiol.* **116**, 2240–2250 (2005).
64. Du, J. *et al.* High-resolution three-dimensional extracellular recording of neuronal activity with microfabricated electrode arrays. *J. Neurophysiol.* **101**, 1671–1678 (2009).
65. Seymour, J. P. & Kipke, D. R. Neural probe design for reduced tissue encapsulation in CNS. *Biomaterials* **28**, 3594–3607 (2007).
66. Polikov, V. S., Tresco, P. A. & Reichert, W. M. Response of brain tissue to chronically implanted neural electrodes. *J. Neurosci. Methods* **148**, 1–18 (2005).
67. Weltman, A., Yoo, J. & Meng, E. Flexible, penetrating brain probes enabled by advances in polymer microfabrication. *Micromachines* **7**, 180 (2016).

Acknowledgements

The research leading to these results has received funding from the Hungarian Brain Research Program Grant (Grant No. 2017-1.2.1-NKP-2017-00002) and from the European Union's Seventh Framework Program (FP7/2007-2013) under grant agreement n°600925 (NeuroSeeker). The research within project No. VEKOP-2.3.2-16-2017-00013 by I. Ulbert was supported by the European Union and the State of Hungary, co-financed by the European Regional Development Fund. The authors are thankful to the Hungarian National Research, Development and Innovation Office for support (PD124175 and PD134196 to R. Fiáth; TUDFO/51757-1/2019-ITM to R. Fiáth and I. Ulbert; K113147, K135837 and NN118902 (CANON project) to Z. Somogyvári).

Author contributions

R.F., P.R. and I.U. designed experiments; R.F., M.D., and P.B. conducted experiments and collected data; R.F., M.D., Z.S., M.B., P.R. and I.U. designed and performed analyses; R.F., Z.S., P.B. and I.U. wrote the manuscript; all authors reviewed the manuscript.

Competing interests

The authors declare no competing interests.

Additional information

Supplementary Information The online version contains supplementary material available at https://doi.org/10.1038/s41598-021-81127-5.

Correspondence and requests for materials should be addressed to R.F.

Reprints and permissions information is available at www.nature.com/reprints.

Publisher's note Springer Nature remains neutral with regard to jurisdictional claims in published maps and institutional affiliations.

Open Access This article is licensed under a Creative Commons Attribution 4.0 International License, which permits use, sharing, adaptation, distribution and reproduction in any medium or format, as long as you give appropriate credit to the original author(s) and the source, provide a link to the Creative Commons licence, and indicate if changes were made. The images or other third party material in this article are included in the article's Creative Commons licence, unless indicated otherwise in a credit line to the material. If material is not included in the article's Creative Commons licence and your intended use is not permitted by statutory regulation or exceeds the permitted use, you will need to obtain permission directly from the copyright holder. To view a copy of this licence, visit http://creativecommons.org/licenses/by/4.0/.

© The Author(s) 2021